Interplay between switching driven by the tunneling current and atomic force of a bistable four-atom Si quantum dot

Shiro Yamazaki,[*,†] Keisuke Maeda,[‡] Yoshiaki Sugimoto,[‡] Masayuki Abe,[¶] Vladimír Zobač,[§] Pablo Pou,[*,‖] Lucia Rodrigo,[‖] Pingo Mutombo,[§] Ruben Pérez,[‖] Pavel Jelínek,[*,‡] and Seizo Morita[†]

†*The Institute of Scientific and Industrial Research, Osaka University, 8-1 Mihogaoka, Ibaraki, Osaka 567-0047, Japan*

‡*Graduate School of Engineering, Osaka University, 2-1, Yamada-Oka, Suita, Osaka 565-0871, Japan*

¶*Graduate School of Engineering Science, Osaka University, 1-1 Machikaneyama, Toyonaka, Osaka, 560-0043, Japan*

§*Institute of Physics, Academy of Sciences of the Czech Republic, Cukrovarnická 10/112, Prague, 162 00, Czech Republic*

‖*Departamento de Física Teórica de la Materia Condensada and Condensed Matter Physics Center (IFIMAC), Universidad Autónoma de Madrid, E-28049 Madrid, Spain*

E-mail: yamazaki@afm.eei.eng.osaka-u.ac.jp; pablo.pou@uam.es; jelinekp@fzu.cz

Atom manipulation process for assembling of Si_4 at RT

Figures 2a and 2b in the main text briefly demonstrated assembling of Si_4 using atom manipulation. Here we show the detail in Fig. S1. Using atom manipulation,[1] we can fabricate Si_4 atom switch at any desired position on the Si(111)-7×7 surface. In this atom-by-atom fabrication process, we can determine the exact number and species of atoms involved in Si_4 atom switch. Figure S1a shows STM image with V_s=-1.0 V at RT where Si_1 atoms are diffusing within half unit cells as indicated by dotted triangles. Half unit cells with diffusing Si_1 atoms look slightly brighter and show faint line noise. Si_1 is confined in the half unit cell by potential barrier of 1 eV at boundary.[2] By bringing a tip near to the boundary vertically as indicated by the black inverted triangle in the inset STM image of Figure S1b, I_t exponentially increases as shown in Fig. S1b (blue curve). Around the closest point (z=0 Å), I_t shows abrupt increase as indicated by the black arrow. It means a Si atom overcomes the energy barrier at the boundary and the Si atom is trapped directly below the tip. During the tip retraction, I_t decreases with the Si atom still trapped by the tip. At certain z indicated by the black arrow (z=1.9 Å), I_t abruptly decreases and returns to original I_t which was observed when the tip was approached. After that, the Si atom is released from the tip apex and starts diffusion in the half unit cell again. As a result, the diffusing Si_1 atom can be laterally manipulated between two half unit cells. Once two Si_1 atoms are placed in half unit cells next to each other, Si_4 is fabricated by self assembling at the boundary as shown in STM image with V_s=-1.0 V in Fig. S1c. Therefore, it has proven that Si_4 is formed by adding only two Si atoms in 7×7 unit cell. The other two Si atoms are provided by native center adatoms of the 7×7 unit as shown in Fig. 2 in the main text.

Atom manipulation and assembly at RT have been carried out using our custom-built AFM/STM.[3] Deflection of metal coated Si cantilevers were detected by an optical interferometer. I_t was detected from the cantilever that was virtually grounded while V_s was applied to a sample.

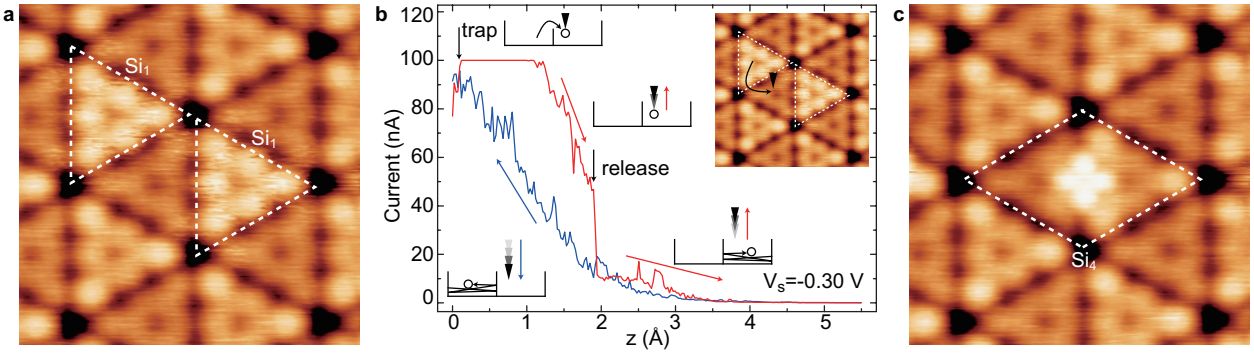

Figure S1: Atom-by-atom assembling of Si_4 using atom manipulation at RT. (a) STM image of the Si(111)-7×7 with diffusing Si monomers (Si_1) as indicated by the dotted triangles with I_t=40 pA and V_s=-1.0 V at RT. (b) Tip-sample distance dependence of I_t with V_s=-0.30 V during tip approaching (blue) and retracting (red) at the boundary between two half unit cells. The tip position is indicated by the inverted triangle in the inset STM image. Schematic side-views showing manipulation processes are depicted in the inset. (c) STM image of Si_4 assembled at the center of the unit cell of Si(111)-7×7 indicated by the dotted rhombus. Acquisition parameters are I_t=40 pA and V_s=-1.0 V. In this fabrication of Si_4 atom switch using atom manipulation, a custom-build interferometer-type RT-AFM was used.[3]

Atom-by-atom assembling of Si_4, Si_5 and Si_6 using atom manipulation at RT

In the main text, only bi-stable symmetric Si_4 QD have been examined. We have also fabricated larger QDs such as Si_5 and Si_6 by repeating atom manipulation of Si_1 as shown in Fig. S2 (see also Movie S1). After about 0.01 ML deposition of Si atom on clean Si(111)-7×7, Si_1 atoms diffusing within half unit cells were observed at RT as shown in Fig. S2a. Si_1 half unit cells are slightly brighter and show line noise as indicated by the dotted triangles in Fig. S2b for eye guide. As shown by the black arrow in Fig. S2b, Si_1 was moved by atom manipulation. As a result, Si_4 was fabricated at the center of the Si(111)-7×7 unit cell (see Fig. S2c). By moving one more Si_1 step-by-step toward the Si_4 unit cell (see the arrows in Fig. S2c and S2d), Si_5 was formed as shown in Fig. S2e. By repeating such processes (see the arrows in Fig. S2f and S2g), finally Si_6 was formed as shown in Fig. S2h. Si_5 and Si_6 are asymmetric Si QDs, unlike symmetric Si_4. Si_5 (Si_6) is apparently compilation of cross Si_4 with one (two) bright Si atom nearby. Si_5 and Si_6

show uni-stable switching behavior at low tip bias at LT, which is not appropriate for switching technology application.

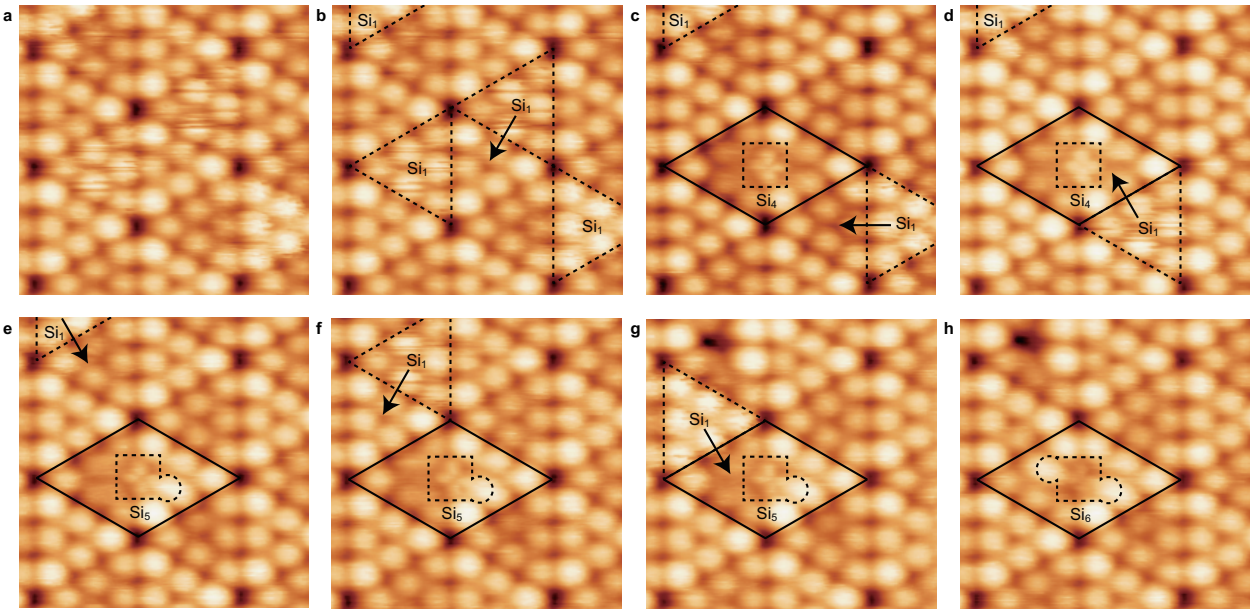

Figure S2: Atom-by-atom assembling of Si_4, Si_5 and Si_6 using atom manipulation at RT. (a)-(h) Sequential STM images with I_t=50 pA and $V_s = -1.5$ V at RT showing atom manipulation of Si_1 for atom-by-atom assembling of Si_4, Si_5 and Si_6. Dotted triangles indicate Si_1 diffusing within half unit cells. Black arrows indicate the directions of Si_1 atom manipulations. Solid rhombuses are target Si(111)-7×7 unit cell that accommodate additional Si_1 atoms. Dotted square, square with circle, and square with two circles are Si_4, Si_5 and Si_6, respectively.

IV curves showing atom switching during bias sweep

Fig. 3 (b)-(k) in main text shows sequential bias dependence of STM images showing threshold bias of atom switching. Threshold bias is also seen by taking IV curves above Si atom of Si_4 as shown in Fig. S3. At low absolute bias ($|V_s| < 0.5$ V), 20 IV curves don't show any switching. At higher bias (0.5 V $< |V_s| < 0.75$ V), IV curves show downward switching between less-dominant U state and dominant D state. At more higher bias ($|V_s| > 0.75$ V), although switching is too fast to see directly, noise increase due to rapid switching is detected. Note that IV curve measured on Si_4 intrinsically involves such switching noise of two state, it is difficult to acquire dI/dV curve or

DOS of each D or U state experimentally.

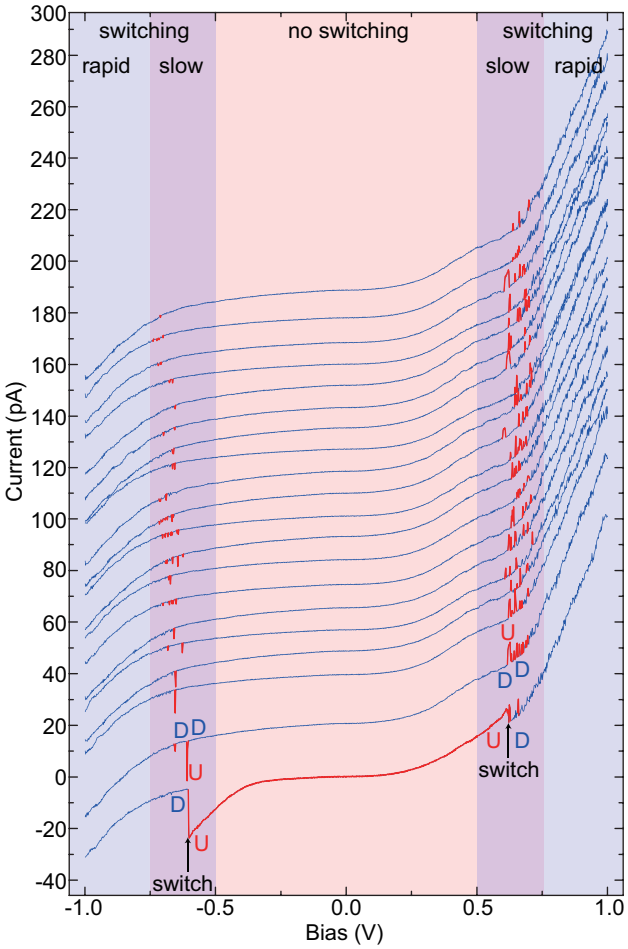

Figure S3: IV curves showing atom switching during bias sweep. 20 IV curves measured above Si atom of Si_4 on unfaulted half side are shown with arbitrary vertical shift. U state and D state are indicated by red and blue color, respectively. IV curves shape show variation depending on timing of switching. The bottom IV curve occasionally keeps U state at around $V_s = 0$ V and shows clear switching between U state and D state as indicated by black arrows. The other IV curves show two-state switching noise between U and D state on purple shaded region, here sweep speed is 10 ms/point. No switching is detected in low absolute bias region as indicated by red shading. In higher absolute bias region as indicated by blue shading, faint noise is detected due to averaged rapid downward switching.

Sequential current dependence of STM images of Si_4

Rate-current plot in Fig. 3m in the main text clearly shows that switching rate linearly increases with increasing of current, indicating one-electron process. This behavior is qualitatively but more

visually seen from sequential current-dependent STM images as shown in Fig. S4. At lowest current (a) 10 pA, the STM image shows 17 times switching during scanning. With increasing current (b) 20 pA and (c) 50 pA, STM images show 33 times and about 60 times switching, respectively, demonstrating linear current dependence. Above (d) 100 pA, it is difficult to count the exact number of switching from STM images. However, it is obvious that number of switching increases from (d) 100 pA to (i) 5.0 nA gradually. As a result, noisy cross-like Si_4 appears due to current-induced downward switching as shown in (i) and schematic view in (j). Note that current dependence is less dramatic than bias dependence (see Fig. 3b-k in the main text), so STM images here do not cover whole range of transformation from frozen Si_4 to complete cross Si_4 in practical current range.

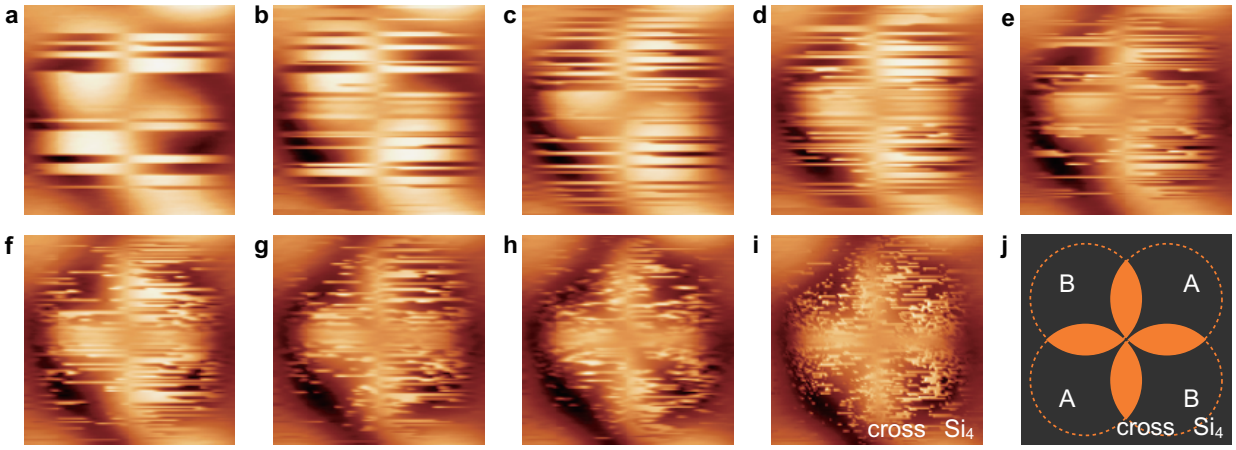

Figure S4: Sequential current dependence of STM images of Si_4. (a)-(i) STM images with increasing I_t; (a) 10 pA, (b) 20 pA, (c) 50 pA, (d) 100 pA, (e) 200 pA, (f) 500 pA, (g) 1.0 nA, (h) 2.0 nA, (i) 5.0 nA with V_s=-0.575 V. Experiments were carried out at 80 K. (j) Schematic drawing of cross-like STM image of Si_4.

Simultaneously acquired AFM and STM images of Si_4

STM images in Figs. 5a-f in the main text show systematic variation of Si_4 appearance from cross shape to square shape with tip-sample distance. Simultaneously acquired constant-hight AFM and STM images support this result and give more details as shown in Fig. S5. At far tip-sample

distance, STM image (f) shows clear cross Si_4 because of current-induced downward switching as explained in main text. At the same tip-sample distance, AFM image (c) does not show any contrast because the short-range force is too small to contribute to atomic resolution image.[3] Therefore, it is evident that switching is dominated by the tunneling current in this tip-sample distance region. At closer distance, STM image (e) shows fuzzy ring-like appearance which could be union of cross and square Si_4. AFM image (b) shows faint halo due to weak attractive force between whole Si_4 and the tip body. At the closest distance, finally AFM image (a) starts showing atomically-resolved image because of the short-range force contribution. At the same time, Si_4 looks square shape. Therefore, the short-range force is essential to explain the square shape of Si_4. At the same tip-sample distance, STM image (d) also shows square Si_4, making sure that difference between cross and square Si_4 is not just due to apparent difference of what AFM and STM record, namely force and current, it is due to real conformation transformation of Si_4.

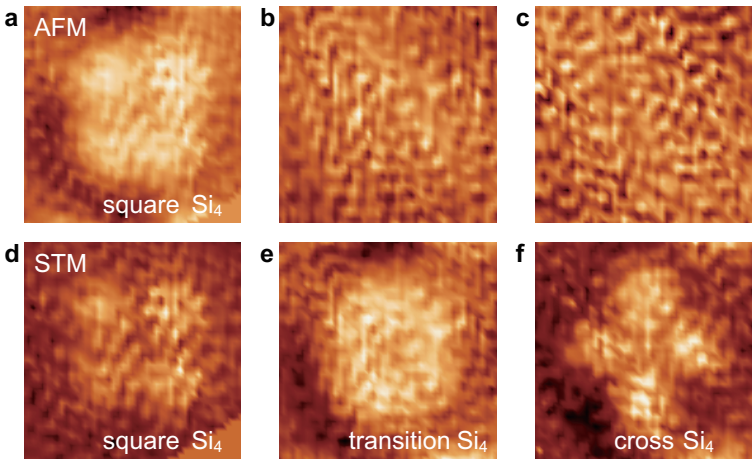

Figure S5: Simultaneously acquired AFM and STM images of Si_4 at RT. (a)-(f) Simultaneously acquired constant-height AFM images (Δf images) (a)-(c) and STM images (I_t images) (d)-(f) with V_s=-0.70 V at RT at various tip-sample distances z [(a)(d); z =0.3 Å, (b)(e); z =1.4 Å, (c)(f); z =3.7 Å].

Transition of switching behavior during tip approach and retraction

Figure 5j in main text shows how upward and downward switching rate vary with the tip-sample distance. There, switching rate is carefully evaluated from telegraph noise measured at several tens different tip-sample distances by fixing the tip height. As shown Fig. S6, alternative simple way reads qualitatively same conclusion as Fig. 5j in a short time. Figure S6a shows tunneling current measured during vertical tip scan on top of a Si atom of Si_4 with V_s=-0.55 V which is slightly higher than switching threshold bias. When tip-sample distance is far (z >0.75 Å), it shows bistable switching between up state and down state. Here, each switching event is still visible and it indicates current induced downward switching. At closer distances (0.0 Å< z < 0.75 Å), each switching event is not detected any more, but it is seen from number of points that resident time of U state gradually increases and D state gradually decreases with tip approach. Finally at short tip-sample distance (z <0.0 Å), resident time of U state become dominant. Resident time ratios are plotted in Fig. S6b. The ratio plots for U and D states cross around z =0.2 Å. At far distance, resident time ratio of D state is slightly less than 1 ($\approx$ 0.8) due to stochastic nature of current induced downward switching. In contrast, at close distance, resident time ratio of U state is exactly 1 due to deterministic nature of force induced upward switching. These behavior is consistent with $\Delta f - z$ curves on top of Si atom of Si_4 shown in Fig. S6b.

Theoretical description of the current induced switching mechanism of the Si_4-QD

The current induced switching mechanism can be explained in terms of the processes that control the desorption induced by electronic transitions (DIET) mechanism.[4] The scenario of subsequent processes, which occur during the switching between two equivalent L and R states of the Si_4-QD is schematically shown on Fig.S7.

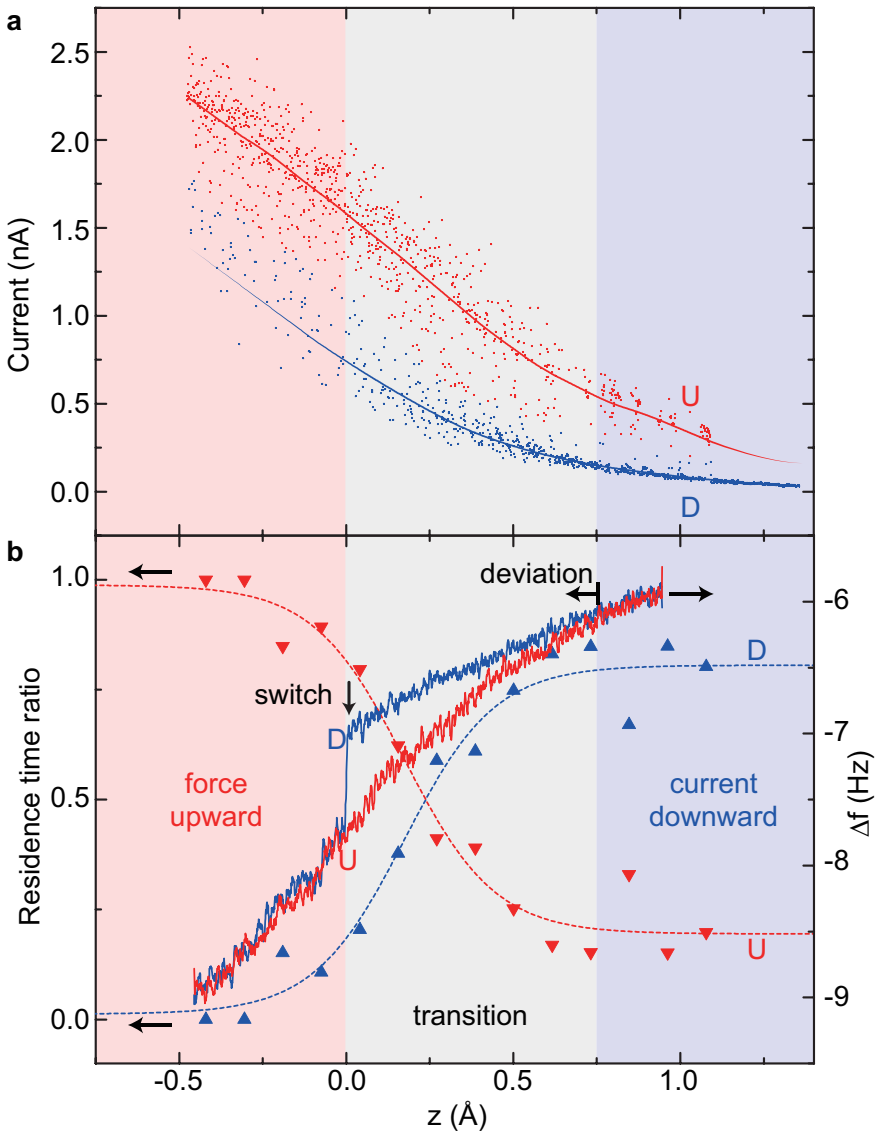

Figure S6: Transition of switching behavior with tip-sample distance. (a) Red and blue dots indicate tunneling current measured by slow tip scan (0.1 ms/point) in the vertical direction on top of a Si atom of Si_4 with V_s=-0.55 V at 80 K. Red (blue) dots are above (bellow) median current of each tip-sample distance, which correspond to up (down) states. Red (blue) solid curve indicates peak position of red (blue) dots distribution. (b) Red inverted triangles (blue triangles) indicate residence time ratio of up (down) state derived by counting number of dots in each finite range of z in (a). Dotted curves are fitted in logistic function $y(z) = a/(1 + e^{-k(z-z_0)}) + b$ for eye guide. Experimental Δf curves (approach and retraction) are also shown by blue and red solid curves. Blue, gray and red shaded region indicate current-induced downward switching, transition, and force-induced upward switching region, respectively. These regions are divided according to switching and deviation point of Δf curves.

Let us consider that the Si_4-QD is initially located in the equilibrium configuration corresponding to the ground state of its potential surface energy (PES^0). When STM tip is located sufficiently close above the Si-tetramer with an applied bias voltage above $\approx$ -0.5 V, the tunneling current can flow between tip apex and Si tetramer atoms. It means, an electron is transferred at certain moment from the localized HOMO state to the probe during the resonant tunneling process leaving behind a hole in the HOMO state (process labeled as 1 on Fig.S7). Consequently the system is temporarily positively charged corresponding to a new potential energy surface (PES^{+1e}). Thus the system is out-of-the-equilibrium and it tends to relax towards the new minima (see process 2 on Fig.S7). In other words, the potential energy is converted into the kinetic energy, ΔE_K^{+1e}, exciting selected vibrational modes. After certain time t_{Q+}, the hole left in the HOMO state recombines with an electron from the Si bulk or surface states and the system becomes neutral again (see process 3 Fig.S7). Thus the system returns to the neutral potential energy surface (PES^0), but again out-of-the-equilibrium position and with an extra kinetic energy ΔE_K^{+1e}. Afterwards the system evolves on the PES^0 and gains even more kinetic energy, ΔE_K^0. If the total kinetic energy, $\Delta E_K^{+1e} + \Delta E_K^0$, acquired during the charging and discharging processes is larger than the activation energy barrier E_b the system can switch to the new minima.

To confirm the validity of the proposed scenario above, we have carried out a set of DFT calculations. First, we have calculated the activation energy barriers for both the neutral and the charged PES, E_b^0 and E_b^{+1} respectively (see Fig.S9). The activation barrier for the charged system, E_b^{+1e} = 0.23 eV, decreases substantially with respect to the neutral system, E_b^0 = 0.44 eV. This is related to the fact that vertical positions and distances between the Si atoms of the tetrameter become almost equal, which facilitates the switching mechanism.

In next, we estimate the mean kinetic energy ΔE_K^{+1e} as the difference between calculated potential energy corresponding to the equilibrium position of the PES^0 and PES^{+1e}, which yields 0.22 eV. This value is comparable to the activation barrier E_b^{+1e} = 0.23 eV. Similarly, we estimated that the mean kinetic energy available for the neutral system after discharging, ΔE_K^0, to be about 0.28 eV. Thus, we see that the total kinetic energy gained in a charging-discharging cycle, $\Delta E_K^0 +$

ΔE_K^{+1e}, could be up to 0.50 eV, which is larger than the activation energy of the neutral system, E_b^0 = 0.44 eV, making the switches possible.

We should note that part of the kinetic energy can be dissipated to surface. Hence it would not contribute to the switching mechanism. To estimate this effect, we have simulated the dynamic of the Si_4-QD on the Si(7x7) surface just after the charging event (see next section for methodological details). On the inset of Fig.S7 we show the evolution of the kinetic energy ΔE_K^{+1e} of the system as a function of time when the system evolves on PES^{+1e} from the equilibrium position corresponding to PES^0. We can immediately see that the system gains a kinetic energy of 0.2 eV within 50 fs, and then it is kept in a vibrational excited state for more than 10^3 fs of our simulation. The DFT calculations (see next section for methodological details) allow us to identify not only the vibrational modes that are excited during the charging/discharging events but also how they overlap with the atomic displacement of the energy minimum path defining the activation barrier (i.e. more overlapping, better the chances to overcome the barrier). In particular, to identify which vibrational mode is the most excited, we projected the initial forces acting on the charged system but in the ground state atomic configuration corresponding to the PES^0. We found only one vibration mode with a strong overlap with the initial force. Thus this is the mode preferentially excited when system is evolving on the PES^{+1e}. What more, it is precisely the same vibration mode responsible for the switching mechanism, see Fig.S11. The discharge of the system from the ground state atomic configuration of the PES^{+1} yields a similar result: the excitation of a vibrational mode that strongly overlaps with the atomic displacements required to overcome the activation barrier (Fig.S10). To summarize, our DFT analysis reveals two important characteristics of vibration modes of the system:

1. The most of the kinetic energy is hold in a single vibrational mode, which is mainly localized on the Si_4-QD (see section devoted to the analysis of the vibration modes). It means, they are only weakly coupled to other vibration modes of the Si(111)-(7×7) surface. This hampers the energy dissipation from the Si_4-QD into the surface.

2. The leading vibration mode coincides with the transition pathway estimated from NEB cal-

culations (see Fig.S11 and Fig.S10). In other words, the most of the kinetic energy is stored to the vibration mode, which leads to the transition between two equivalent states of the Si_4-QD.

It is also important to analyze a characteristic charging time t_T, which the system spends between two subsequent resonant tunneling processes. The time t_T can be estimated directly from the tunneling current. Namely, in our experiment I_t =100 pA corresponds to time $t_T = 1.6$ ns between two consecutive electrons pass through the tunneling junction. We immediately see that the characteristic charge time t_T is much longer than the relaxation time τ of the system corresponding to the principal vibration mode estimated as $\omega = 8.72$ THz (i.e. $\tau \approx 0.1$ps) (see the section Vibrational modes) or similarly to the variation of the kinetic energy shown on the inset of Fig.S7.

In summary, our DFT calculations show that (i) the energy barriers; (ii) the available kinetic energy gained during the charging/discharging cycle; (iii) the excited vibrational modes during this cycle and (iv) the decoupling between the atomic movements of the Si_4 and the Si surface make the current induced switching mechanism feasible.

Total energy DFT calculations

To simulate the Si_4-QD system we have used a 6-layer slab (3 bilayers) of the Si(111)-7x7 on top of which two extra Si atoms were included. With these two extra atoms along with two center adatoms of the Si(111)-7x7 cell the characteristic tetramer structure was obtained. Total number of atoms was 349 atoms including the hydrogen atoms used to passivate the last layer of Si atoms. We performed the structural relaxation using the tight-binding ab initio FIREBALL code within the local density approximation formalism.[5] The code used an optimized spatially-confined pseudo-atomic basis set.[6] Here we used an spd basis set to describe the Si atoms and an extended double basis set for the hydrogen atoms. The pseudo-atomic basis functions had the following cutoff radii: R(Si,s)=4.8 a.u, R(Si,p)=5.4, R(Si,d)=5.2 a.u., and R(H,s,s*)=4.5 a.u. The calculations were restricted to the Γ point of the first surface Brillouin zone. The bottom Si atomic layer as well as

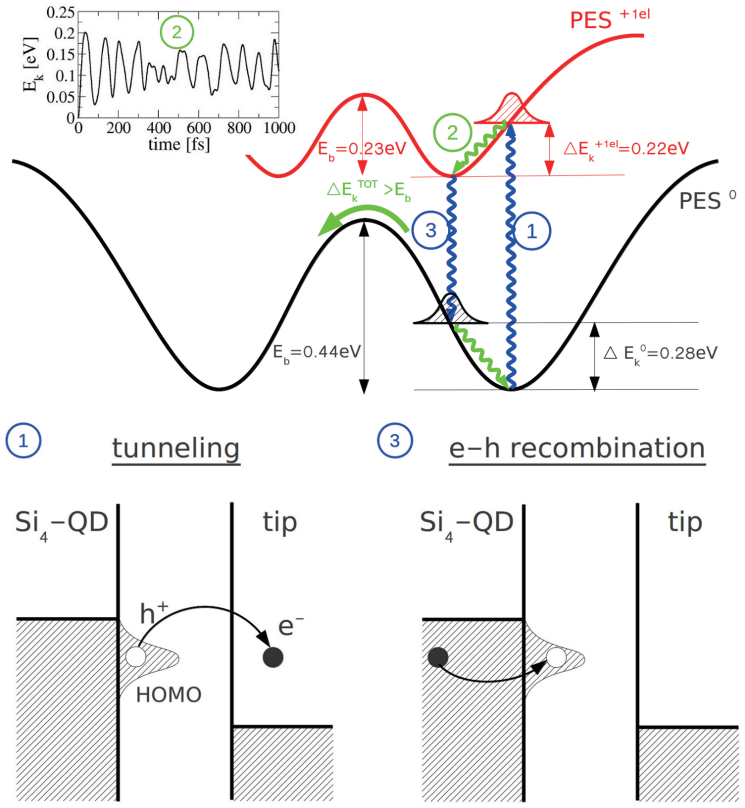

Figure S7: Schematic representation of different processes leading to the current induced switching mechanism due to subsequent transition between two different potential energy surfaces (PES^0 and PES^{+1e}) as a consequence of a withdrawal and subsequent input of an electron into the localized HOMO state in the Si_4-QD. The characteristic activation energy barriers and gained kinetic energies for both PES^0 and PES^{+1e} are schematically shown.

the hydrogen layer were kept fixed during the geometry optimization while all other atoms were allowed to relax freely into their equilibrium positions. The criterion for terminating the relaxation was that maximal forces on free atoms had to be below 0.05 eV/Å and the change of total energy between subsequent iterations had to be smaller than 10^{-4} eV per unit cell.

Beside the large scale Si-tetramer on the Si(111)-7x7 surface, we also use a small Si-cluster to make constrain DFT molecular dynamics computationally less demanding. Namely, we use a Si-cluster consisting of 16 Si atoms and 18 H atoms built from the full Si(111)-7x7 system and passivated with the needed H atoms (see Fig.S8). The cluster reproduces very well atomic, electronic and mechanical properties of the Si_4-QD system. For example the activation energy barriers between different tetramer states calculated for the Si-cluster are very similar to those calculated with the Si-tetramer on the Si(111)-7x7 surface as shown on Fig.S9.

In addition, the geometry optimization, electronic properties, activation energy barriers and vibrational modes calculations were also performed using the plane-wave pseudopotential package VASP[7] (with Vanderbilt ultrasoft pseudopotentials,[8] PBE[9] and a cutoff energy of 300 eV) to corroborate the Fireball results.

Constrained DFT molecular dynamics of the Si_4-QD out-of-equilibrium

We used constrained DFT molecular dynamics implemented within FIREBALL code to study the time evolution of the Si_4-QD system out-of-equilibrium on both the ground PES^0 and charged potential energy surface PES^{+1e}. To mimic the dynamics of the charged Si_4-QD system evolving on PES^{+1e} we subtracted one electron from the HOMO Kohn Sham (KS) state in the calculations. To achieve this effect, we use the projection of the KS orbitals from the previous step on the KS orbitals in the current step, identifying whether the orbitals order was changed. Thus, the desired occupation of the KS states can be imposed during the time evolution. The molecular dynamics of the system was studied by an isokinetic ensemble at a temperature of 300 K, the temperature was held by velocity rescaling thermostat. The nuclei were propagated classically according to Newton equations by the Velocity Verlet algorithm with a time step of 0.25 fs. The evolution of the system

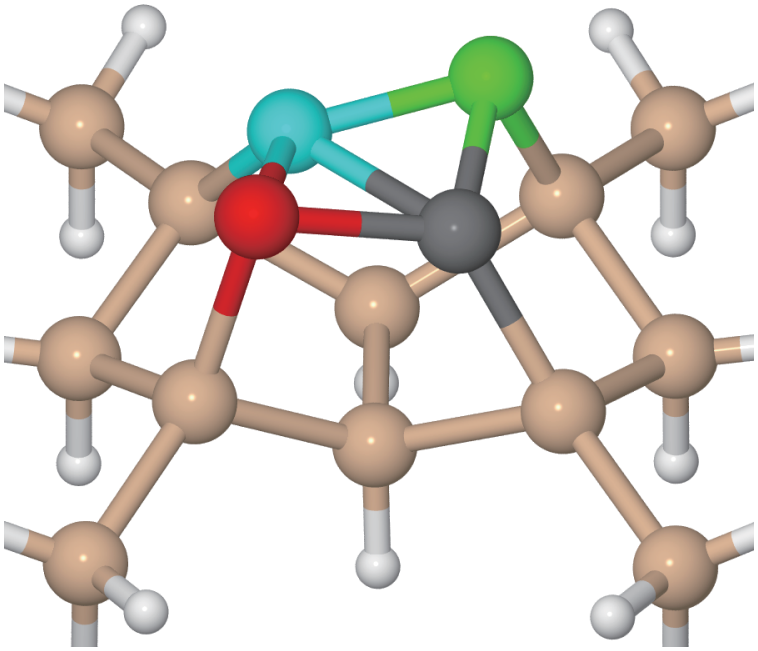

Figure S8: Detail view of the optimized atomic structure of the Si-cluster used for the efficient constrained DFT molecular dynamics simulations.

on the PES^{+1e} is shown on inset of Fig.S7.

NEB calculations

The Nudged Elastic Band (NEB) method[10] was used in order to reveal the transition pathway between two stable configurations of the Si_4-QD. We used 16 images to sample the phase space, a spring constant of 1 and a displacement tolerance of 0.03 Å. For this calculations the force and energy convergence criteria used were 0.03 eV/Å and 0.003 eV respectively. The initial configurations of the images were sampled linearly among the initial and final state. The optimization was performed using the Verlet algorithm with a 0.1 fs time step.

With this method we have calculated the energy barriers for the Si_4-Si(111)-7x7 system and for the cluster in both neutral (PES^0) and positively charged systems (PES^{+1e}). Results are shown in Fig.S9. We have also benchmarked the obtained activation barriers with VASP. The activation energy barriers obtained with VASP are very similar to the values calculated with FIREBALL (see

Fig.S9).

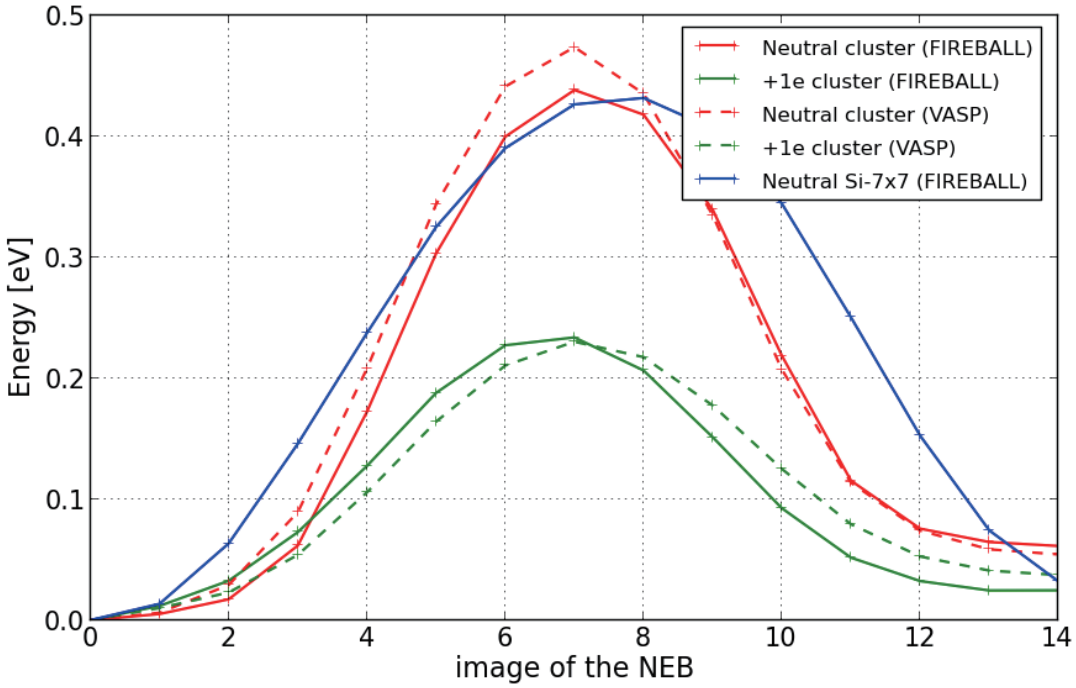

Figure S9: Comparison of the activation energy barriers of the cluster and the Si(111)-7x7 for the ground (PES^{0}) and charge (PES^{+1e}) states calculated with both Fireball and VASP code.

Vibrational modes

We analyze the characteristic vibrational modes of the Si_4-QD system using the dynamical matrix approach implemented in FIREBALL code. The dynamical matrix was calculated by numerical differentiation of forces with a finite displacement of atoms 0.03 Å. To identify the leading modes responsible for the transition between two ground states, we perform the projection of the NEB transition pathways onto all vibration modes for the Si_4-QD on the ground (PES^{0}) and charged (PES^{+1e}) potential energy surface. The calculations revealed a dominant characteristic mode, which is mostly responsible for the transition between L and R configuration states of the Si_4-QD. What more the leading vibration mode is very similar for both the ground (PES^{0}) and charged (PES^{+1e}) potential energy surfaces (see Fig.S10 and Fig.S11). We also checked the validity of the calculated vibration spectra with VASP code.

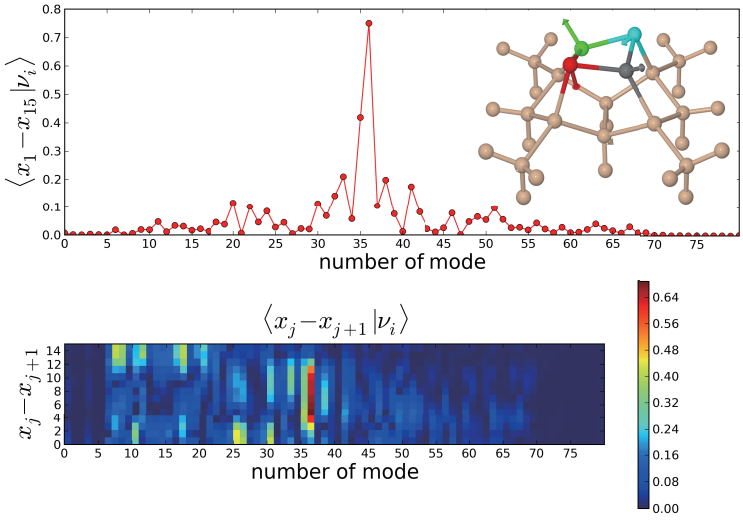

Figure S10: Top: Projection of modes onto characteristic NEB displacement defined as vector pointing from the first towards the last image of the NEB for the neutral Si-cluster (PES^0). The inset images shows vibration mode no. 37, which matches the best the NEB trajectory. Down: Projection of the modes on the NEB displacement between neighboring NEB images x_j for the neutral Si-cluster.

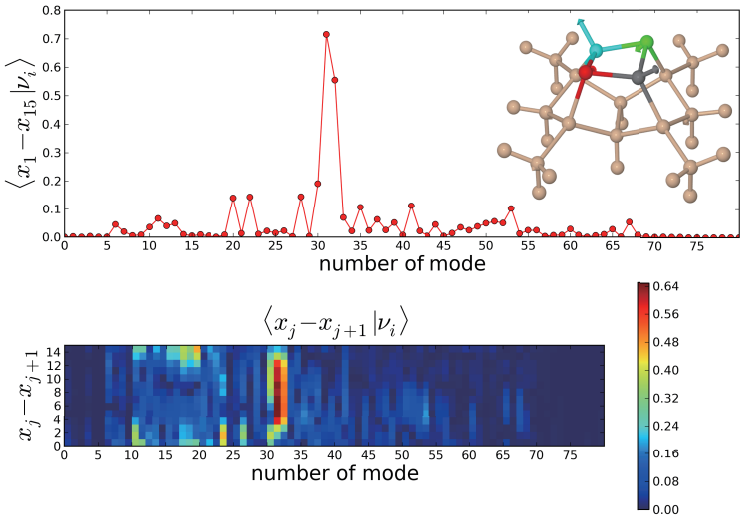

Figure S11: Top: Projection of modes onto characteristic NEB displacement defined as vector pointing from the first towards the last image of the NEB for the charged Si-cluster PES^{+1e}. The inset images shows vibration mode no. 31, which matches the best the NEB trajectory. Down: Projection of the modes on the NEB displacement between neighboring NEB images x_j for the charged Si-cluster.

STM calculations

To understand experimental STM images of the Si-tetramer structure we performed STM simulations using the Green's function formalism.[11] The Green's functions are calculated using a local basis set Hamiltonian corresponding to fully optimized atomic structure of the Si_4-Si(111)-7x7 obtained from FIREBALL code (see the total energy DFT calculations). We used H3 Si-tip[12] attached to a metal slab. All the STM simulations were calculated in the constant-current mode for a bias voltage of -0.4V, η=0.05 and a tip-sample distance of 6Å.

FM-AFM calculations

We have performed quasi-static approach force-versus-distance calculations (i.e. at 0 K) using a silicon H3 tip model.[12] In a way that the tip was gradually moved towards the surface in steps of 0.25 Å along the surface normal. At every such steps all surface and tip atoms (except for the bottom layer of the slab and the base part of the tip) were allowed to relax to their ground-state configuration, fulfilling the convergence criteria specified above. The total short-range tip-sample forces were then determined as a sum of the final forces acting on the fixed atoms of the tip. The 5 Å range of tip-sample distances covers both attractive and repulsive regions, which is important for the force switching mechanism.

Figure S12 shows the calculated force curves (upper panel) and vertical position of each Si atom of the Si_4-QD with different tip-surface distances (lower panel). The black force curve is the short-range force when the tip approaches above down Si atom (black ball in the inset) while the red curve is retraction curve (same as the theoretical curves in Fig. 4g in the main text). Lower panel displays the vertical relaxation of four Si atoms forming the tetramer along tip approach and subsequent retraction. The color of the plots corresponds to each Si atom with the same color in the inset. Solid (dashed) lines connecting plots represent approach (retraction) data. We can extract the procedures of atom switch in detail from the plots. The vertical relaxations reveal detail mechanism of the force-induced switching mechanism.

Figure S13 shows the data set similar to Fig.S12, but the tip approaches an upper Si atom shown by the green ball. In this case, the atom located underneath of tip apex does not switch as can be seen in the lower panel.

The total energy of the system is plotted as a function of the tip-surface distance in Fig.S14, which corresponds to Fig.S12. When the tip approaches the down Si atom, this atom jumps to contact to the tip at z=0. At this moment, energy gain caused by the tip approach is around -0.4 eV, which is remarkably close to the barrier reduction for the atom switch as duplicated in the inset from Fig. 5k in the main text.

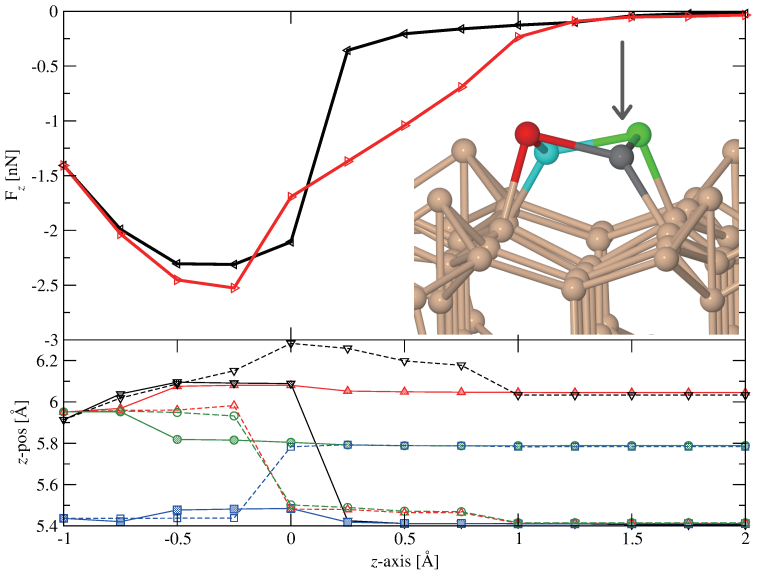

Figure S12: Upper panel shows calculated $F-z$ curves over D-site of the Si_4-QD during approach (black line) and retraction (red line) of probe. Lower panel displays vertical relaxation of four Si atoms of the Si_4-QD during approach (solid line) and retraction (dashed line) of probe. Each atom can be identified by color scale from inset figure, which show the initial atomic structure of the Si_4-QD; black dart indicates place where tip was approached.

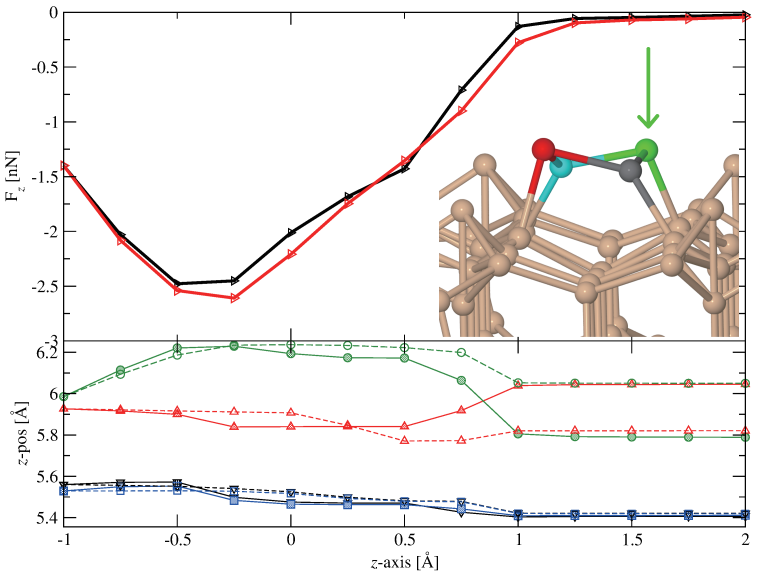

Figure S13: Upper panel shows calculated $F - z$ curve over U-site of the Si_4-QD during approach (black line) and retraction (red line) of probe. Lower panel displays vertical relaxation of four Si atoms of the Si_4-QD during approach (solid line) and retraction (dashed line) of probe. Each atom can be identified by color scale from inset figure, which show the initial atomic structure of the Si_4-QD; green dart indicates place where tip was approached.

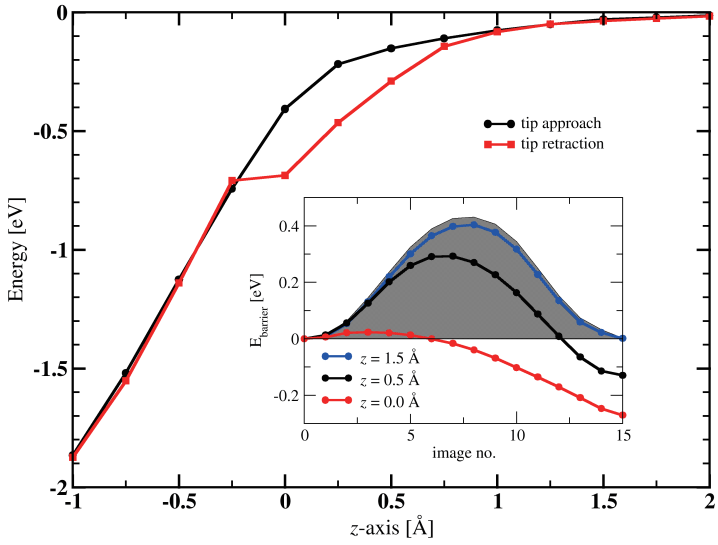

Figure S14: Variation of the total energy with respect to the initial configuration of the Si_4-QD along the tip approach (black) and retraction (red). Inset figure shows calculated activation energy barrier for switching between L (left) and R (right) state.

References

1. Sugimoto, Y.; Yurtsever, Y.; Hirayama, N.; Abe, M.; Morita, S. Mechanical gate control for atom-by-atom cluster assembly with scanning probe microscopy. *Nat. Commun.* **2014**, *5*, 4360.

2. Chang, C. M.; Wei, C. M. Diffusion of an adsorbed Si atom on the Si(111)-(7x7) surface. *Phys. Rev. B* **2003**, *67*, 033309.

3. Sugimoto, Y.; Nakajima, Y.; Sawada, D.; Morita, K.; Abe, M.; Morita, S. Simultaneous AFM and STM measurements on the Si(111)-(7x7) surface. *Phys. Rev. B* **2010**, *81*, 245322.

4. Betz, G.; Varga, P. *Desorption induced by electronic transitions, DIET IV: proceedings of the fourth international workshop, Gloggnitz, Austria, October 2-4*; Springer-Verlag, 1990.

5. Lewis, J. P.; Jelínek, P.; Ortega, J.; Demkov, A. A.; Trabada, D. G.; Haycock, B.; Wang, H.; Adams, G.; Tomfohr, J. K.; Abad, E. *et al.* Advances and applications in the FIREBALLab initio tight-binding molecular-dynamics formalism. *physica status solidi (b)* **2011**, *248*, 1989–2007.

6. Basanta, M. A.; Dappe, Y. J.; Jelinek, P.; Ortega, J. Optimized Atomic-like Orbitals for First-principles Tight-binding Molecular Dynamics. *Comp. Mat. Sci.* **2007**, *39*, 759–766.

7. Kresse, G.; Furthmüller, J. Efficient iterative schemes for ab initio total-energy calculations using a plane-wave basis set. *Phys. Rev. B* **1996**, *54*, 11169–11186.

8. Vanderbilt, D. Soft self-consistent pseudopotentials in a generalized eigenvalue formalism. *Phys. Rev. B* **1990**, *41*, 7892.

9. Perdew, J. P.; Burke, K.; Ernzerhof, M. Generalised gradient approximation made simple. *Phys. Rev. Lett.* **1996**, *77*, 3865.

10. Henkelman, G.; Jónsson, H. Improved Tangent Estimate in the Nudged Elastic Band Method for Finding Minimum Energy Paths and Saddle Points. *J. Chem. Phys.* **2000**, *113*, 9978–9985.

11. Blanco, J. M.; Flores, F.; Pérez, R. STM-theory: Image potential, chemistry and surface relaxation. *Prog. Surf. Sci.* **2006**, *81*, 403–443.

12. Pou, P.; Ghasemi, S. A.; Jelinek, P.; Lenosky, T.; Goedecker, S.; Perez, R. Structure and Stability of Semiconductor Tip Apexes for Atomic Force Microscopy. *Nanotechnology* **2009**, *20*, 264015.